

Detection of the static and kinetic pinning of domain walls in ferromagnetic nanowires

Sung-Min Ahn,¹ Kyoung-Woong Moon,¹ Dong-Hyun Kim,² and Sug-Bong Choe^{1,a)}

¹Department of Physics, Seoul National University, Seoul 151-742, Republic of Korea

²Department of Physics, Chungbuk National University, Cheongju 361-763, Republic of Korea

(Received 24 July 2009; accepted 24 September 2009; published online 13 October 2009)

Two distinct pinning mechanisms named as kinetic and static pinning of magnetic domain wall (DW) are experimentally resolved. Both the pinning situations are realized at an artificial notch on U-shaped Permalloy nanowires, depending on the initial DW states, moving or pinned. The kinetic depinning field—a critical field for a moving DW to be trapped at a notch—is revealed to be distinguishably smaller than the static depinning field—a critical field to depin a trapped DW at the notch. Based on one-dimensional collective model, the discrepancy is explained by the tilting angle of the moving DW. © 2009 American Institute of Physics. [doi:10.1063/1.3248220]

Magnetic domain wall (DW) in nanowires has been focused due to the promising applications such as magnetic logic and memory devices.^{1,2} Since the DW carries the logic and/or memory information, it is essential to precisely manipulate the DW positions, practically by introducing artificial constraints such as notches.^{3–7} The DW shift between notches is accomplished by two successive processes: (i) depinning of a trapped DW from a notch and (ii) pinning of a moving DW at another notch. Thus, one has to distinguish two pinning mechanisms depending on the initial states of DWs, either trapped or moving. We denote the former and the latter as the static and kinetic pinning processes, respectively. All the previous studies have examined only the static pinning process but the kinetic pinning process has not been experimentally demonstrated yet, despite a micromagnetic prediction.⁸ In this letter, we present an experimental proof that the kinetic pinning process is distinct from the static pinning process, by exhibiting the noticeably different strengths of the depinning fields.

For this study, 20-nm-thick Ni₈₁Fe₁₉ films are deposited onto Si(100) substrates by dc-magnetron sputtering under 2 mTorr Ar pressure. U-shaped nanowire structures are then patterned by the electron beam lithography followed by reactive ion etching. Several structures are realized with different widths—350, 620, and 1170 nm, respectively. The secondary electron microscope image of the 620-nm-wide nanowire structure is depicted in Fig. 1. A notch is placed in the middle of the structure as designated by the arrows in the figure. The notch is composed of two symmetric triangles, which exhibits a unique static depinning field⁹ irrespective of the DW chirality and propagation direction,¹⁰ unlikely to the single notches exhibiting complex pinning mechanisms.¹¹ The notch depths are 90, 170, and 350 nm, respectively, for each nanowires, which are roughly 30% of the nanowire widths.

The DW propagation along the nanowires is then measured by a longitudinal Kerr effect measurement system with a laser spot of ~500 nm in diameter by use of a 405 nm laser and an objective lens of the numerical aperture 0.9. The laser spot is placed at the left side of the notch as shown by the circle in Fig. 1. The measurement scheme is as follows.

(1) An external magnetic field H_{sat} (~400 Oe) is first applied to the structure with an angle θ (~60°) and thus, a DW is created at the left corner after turning-off the magnetic field. (2) The magnetic field is then applied rightward up to H_{sweep} in the horizontal direction, to bring the DW from the left corner to the right. (3) Finally the magnetic field is swept leftward to bring the DW back to the left corner.

Depending on the strength of H_{sweep} , the DW is brought to the different positions as pointed by **A**, **B**, **C**, and **D**, respectively in Fig. 1, which in turn generates four different hysteresis loops. We denote three depinning fields as the depinning field $H_{\text{left}}^{\rightarrow}$ from the position **A**, the depinning field $H_{\text{notch}}^{\rightarrow}$ from the position **B**, and the depinning field $H_{\text{notch}}^{\leftarrow}$ from the position **C**. The values of the depinning fields are listed in Table I.

In Regime I with $H_{\text{sweep}} < H_{\text{left}}^{\rightarrow}$, no change in the Kerr signal is observed as shown in Fig. 2(a), since the DW is kept pinned at the natural edge roughness of the left corner. Note that $H_{\text{left}}^{\rightarrow}$ is set to be a small value by adjusting θ and H_{sat} .

In Regime II, the DW is depinned from the left corner and then, pinned at the notch. There are two possible pinning positions, either the left or the right sides of the notch, as designated by the positions **B** and **C**, respectively. We thus classify Regime II into two subregimes. For Regime IIa with $H_{\text{left}}^{\rightarrow} < H_{\text{sweep}} < H_{\text{notch}}^{\leftarrow}$, the DW is pinned at **B**. By reversing the sweeping field, the DW is depinned leftward under the

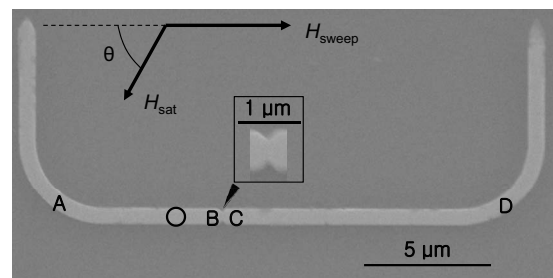


FIG. 1. Secondary electron microscope image of 620-nm-wide Permalloy U-shaped nanowire structure with a notch. The circle on the wire shows the position of the probing laser spot for the Kerr effect measurement. Typical pinning positions are designated by **A**, **B**, **C**, and **D**, respectively. The inset shows the high resolution image of the notch. The arrows indicate the magnetic field directions of H_{sat} and H_{sweep} .

^{a)}Electronic mail: sugbong@snu.ac.kr.

TABLE I. The leftward and rightward depinning fields of the notches in several nanowires with different widths. The field unit is oersted. Note that \times indicates that the depinning is forbidden since $H_{\text{notch}}^{l\rightarrow} > H_{\text{notch}}^{r\rightarrow}$.

	350 nm	620 nm	1170 nm
$H_{\text{left}}^{\rightarrow}$	70.0 ± 4.0	35.6 ± 0.4	20.0 ± 4.0
$H_{\text{notch}}^{l\rightarrow}$	252.0 ± 4.0	66.8 ± 0.4	44.0 ± 4.0
$H_{\text{notch}}^{r\rightarrow}$	\times	146.8 ± 0.4	98.0 ± 2.0
$H_{\text{right}}^{\leftarrow}$	102.7 ± 3.5	34.6 ± 4.2	12.9 ± 3.1
$H_{\text{notch}}^{r\leftarrow}$	\times	96.9 ± 6.3	58.1 ± 7.0
$H_{\text{notch}}^{l\leftarrow}$	128.0 ± 2.4	67.5 ± 3.5	15.1 ± 0.7

depinning field $H_{\text{notch}}^{l\leftarrow}$, as plotted in Fig. 2(b). On the other hand, in Regime IIb with $H_{\text{notch}}^{l\rightarrow} < H_{\text{sweep}} < H_{\text{notch}}^{r\rightarrow}$, the DW is pinned at **C** and then, depinned leftward under $H_{\text{notch}}^{r\leftarrow}$ as shown in Fig. 2(c). This regime appears only when $H_{\text{notch}}^{l\rightarrow} < H_{\text{notch}}^{r\rightarrow}$. These two depinning fields can be tuned independently by adjusting the depth and the slope of the notch.¹² Note that these two leftward depinning fields $H_{\text{notch}}^{l\leftarrow}$ and $H_{\text{notch}}^{r\leftarrow}$ are governed by the static pinning process, since the DWs in these cases are initially trapped at the notch.

The kinetic process is realized in Regime III with $H_{\text{notch}}^{r\rightarrow} < H_{\text{sweep}}$. In this regime, the hysteresis loop shown in Fig. 2(d) exhibits much smaller depinning field compared with those in Regime II. In this regime, H_{sweep} is strong enough to bring the DW to the position **D**. By sweeping a negative magnetic field, the DW is depinned from **D** under the depinning field $H_{\text{right}}^{\leftarrow}$. Note that $H_{\text{right}}^{\leftarrow}$ is much smaller than $H_{\text{notch}}^{l\leftarrow}$ and $H_{\text{notch}}^{r\leftarrow}$ as listed in Table I. However, it is quite interesting to see that once depinned from the right corner, the kinetic DW continues to pass through the notch. One thus conjectures that the kinetic DW experiences much smaller pinning field in comparison with the static DW.

Figure 3 summarizes the depinning fields with respect to the strength of H_{sweep} . Note that H_{sweep} is the maximum field swept horizontally to the rightward; the maximum field to the leftward is fixed to -300 Oe. Each symbol is obtained by averaging more than ten times repeated measurements. All the nanowires with different widths, (a) 620, (b) 350, and (c) 1170 nm, exhibit basically the same behavior. It is clearly

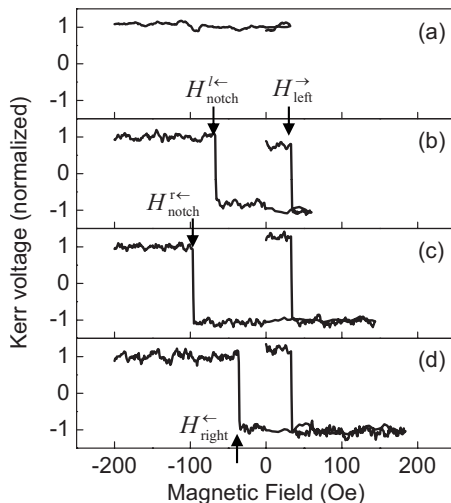


FIG. 2. Longitudinal Kerr hysteresis loops of the nanowire structure shown in Fig. 1. Depending on the strength of H_{sweep} , typical loops are shown for the four different regimes: (a) Regime I, (b) Regime IIa, (c) Regime IIb, and (d) Regime III, respectively.

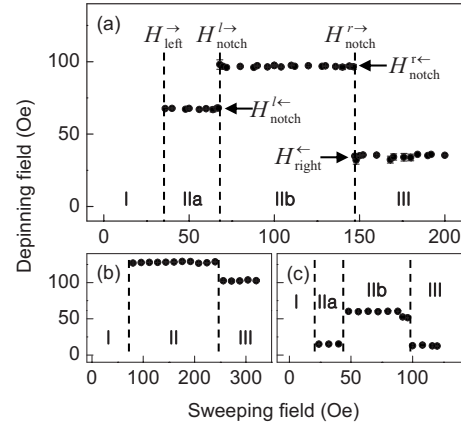


FIG. 3. Depinning fields with respect to H_{sweep} for several nanowire structures with different widths: (a) 620, (b) 350, and (c) 1170 nm, respectively.

seen from the plots that there exist three (or four) regimes with distinct depinning fields. The depinning field inside each regime is almost constant irrespective of H_{sweep} . The threshold values in the abscissa are the rightward depinning fields i.e., $H_{\text{left}}^{\rightarrow}$, $H_{\text{notch}}^{l\rightarrow}$, and $H_{\text{notch}}^{r\rightarrow}$ for each position as denoted in the plot. The ordinate corresponds to the leftward depinning fields i.e., $H_{\text{notch}}^{l\leftarrow}$, $H_{\text{notch}}^{r\leftarrow}$, and $H_{\text{right}}^{\leftarrow}$. The values are listed in Table I.

One-dimensional collective model¹³ of the DW is adopted to explain the present results. In this model, by assuming a rigid DW, the DW motion is described by the two parameters, the position q and the tilting angle ψ of the magnetization inside the DW. The equation of motion is then given by

$$\frac{1 + \alpha^2}{\alpha\gamma\Delta} \dot{q} = H - \frac{1}{2M_S} \varepsilon'(q) + \frac{1}{\alpha} \frac{H_K}{2} \sin(2\psi),$$

$$\frac{1 + \alpha^2}{\gamma} \dot{\psi} = H - \frac{1}{2M_S} \varepsilon'(q) - \alpha \frac{H_K}{2} \sin(2\psi), \quad (1)$$

where α is the Gilbert damping constant, γ is the gyromagnetic ratio, Δ is the DW width, M_S is the saturation magnetization, H is the strength of the external magnetic field, and H_K is the shape anisotropy field of the DWs. The energy function $\varepsilon(q)$ describes the pinning potential around the notch and ε' denotes $\partial\varepsilon/\partial q$.

For the static pinning case, the DW is initially placed at the position q_0 for minimum potential energy $\varepsilon(q_0)$ and the zero tilting angle, $\psi=0$. With gradual increment of H , the DW is gradually shifted inside the potential to the position q_H for $\varepsilon'(q_H)=2M_S H$ with maintaining $\psi=0$. The DW is finally depinned from the notch, just when the external magnetic field exceeds the maximum pinning field. The static depinning field is thus given by $H_{\text{dp}}^{\text{Static}} = [\varepsilon']_{\text{MAX}}/2M_S$. On the other hand, for the kinetic pinning case, the DW is initially moving. Let us consider that it moves in $+q$ direction with positive H . For this case the DW has nonzero tilting angle ψ . Thus, the DW can stop (i.e., $\dot{q}=0$ and $\dot{\psi}=0$) only when the condition $H < H_{\text{dp}}^{\text{Static}} - H_K \sin(2\psi)/2\alpha$ holds for all the time in the whole notch area. The DW thus has a chance to pass through the notch under a field smaller than $H_{\text{dp}}^{\text{Static}}$. Note that the term $\sin(2\psi)$ initially has a positive value for a field below the Walker breakdown field¹⁴ or has an alternating value between ± 1 above the Walker breakdown field.

For the simplest case of the pinning potential as given by

$$\varepsilon(q) = \begin{cases} 0, & \text{for } q \leq 0 \\ 2M_s H_0 q, & \text{for } 0 \leq q \leq \delta. \\ 2M_s H_0 \delta, & \text{for } q \geq \delta \end{cases} \quad (2)$$

Equation (1) can be analytically solved for a small tilting angle i.e., $\sin(2\psi) \cong 2\psi$. Here, δ is the lateral size of the pinning potential and H_0 is the pinning field. The solution is

$$q(t) = \frac{\gamma\Delta}{\alpha}(H - H_0)t + \frac{\Delta}{\alpha^2 H_K} \left[1 - \exp\left(-\frac{\alpha\gamma}{1 + \alpha^2} H_K t\right) \right],$$

$$\psi(t) = \frac{H_0}{\alpha H_K} \exp\left(-\frac{\alpha\gamma}{1 + \alpha^2} H_K t\right) - \frac{H_0 - H}{\alpha H_K}, \quad (3)$$

for $0 \leq q \leq \delta$. The maximum value of $q(t)$ is given by

$$q_{\max} = \frac{\Delta}{\alpha^2 H_K} \left\{ H_0 + (1 + \alpha^2)(H_0 - H) \left(\log \left[1 + \alpha^2 \frac{H_0 - H}{H_0} \right] - 1 \right) \right\}. \quad (4)$$

Under the approximation that $1 + \alpha^2 \cong 1$ since $\alpha \ll 1$, it becomes

$$q_{\max} \sim \frac{\Delta}{\alpha^2 H_K} \sum_{n=1}^{\infty} \frac{(H/H_0)^{n+1}}{n(n+1)}. \quad (5)$$

The DW is pinned if $q_{\max} \leq \delta$, otherwise it is depinned from the notch. Therefore, the kinetic depinning field $H_{\text{dp}}^{\text{kinetic}}$ is determined by the condition $q_{\max} = \delta$. Expanding the summation in Eq. (5) up to $n=4$, the valid root for the kinetic depinning field is finally obtained as

$$H_{\text{dp}}^{\text{kinetic}} \sim \alpha \sqrt{2\delta H_K H_0 / \Delta} - \alpha^2 \delta H_K / 3\Delta + O(\alpha^3). \quad (6)$$

In contrast, the static depinning field in this case is readily obtained as $H_{\text{dp}}^{\text{static}} = H_0$. In Permalloy nanowires, the values

of the parameters in Eq. (6) are typically in the orders of magnitudes— $\alpha \sim 0.01$, $\delta \sim \Delta$, and $H_K \sim$ a few kilo-oersted.¹³ Therefore, the kinetic depinning field of the notches in our samples is estimated to be about a few oersted, which is significantly smaller than the static depinning field of a few tens of oersted. In our experiments, we prove the existence of the two distinct pinning mechanisms by demonstrating that the kinetic depinning field is smaller than the static depinning field. The upper bound of the kinetic depinning field is given in the experiments and the exact kinetic depinning field measurement can probe the realistic pinning potential profiles.

This study was supported by the KOSEF through the NRL program (Grant No. R0A-2007-000-20032-0).

- ¹S. S. P. Parkin, M. Hayashi, and L. Thomas, *Science* **320**, 190 (2008).
- ²D. A. Allwood, G. Xiong, C. C. Faulkner, D. Atkinson, D. Petit, and R. P. Cowburn, *Science* **309**, 1688 (2005).
- ³D. A. Allwood, G. Xiong, and R. P. Cowburn, *Appl. Phys. Lett.* **85**, 2848 (2004).
- ⁴M. T. Bryan, T. Schrefl, and D. A. Allwood, *Appl. Phys. Lett.* **91**, 142502 (2007).
- ⁵M. Tsoi, R. E. Fontana, and S. S. P. Parkin, *Appl. Phys. Lett.* **83**, 2617 (2003).
- ⁶J. Grollier, P. Boulenc, V. Cros, A. Hamzi, A. Vaurès, A. Fert, and G. Faini, *Appl. Phys. Lett.* **83**, 509 (2003).
- ⁷C. K. Lim, T. Devolder, C. Chappert, J. Grollier, V. Cros, A. Vaurès, A. Fert, and G. Faini, *Appl. Phys. Lett.* **84**, 2820 (2004).
- ⁸S.-M. Ahn, D.-H. Kim, and S.-B. Choe, *IEEE Trans. Magn.* **45**, 2478 (2009).
- ⁹S.-B. Choe, *J. Magn. Magn. Mater.* **320**, 1112 (2008).
- ¹⁰L. K. Bogart and D. Atkinson, *Phys. Rev. B* **79**, 054414 (2009).
- ¹¹D. Atkinson, D. S. Eastwood, and L. K. Bogart, *Appl. Phys. Lett.* **92**, 022510 (2008).
- ¹²K.-J. Kim, C.-Y. You, and S.-B. Choe, *J. Magn.* **13**, 136 (2008).
- ¹³L. Thomas, M. Hayashi, X. Jiang, R. Moriya, C. Rettner, and S. S. P. Parkin, *Nature (London)* **443**, 197 (2006).
- ¹⁴A. Mougín, M. Cormier, J. P. Adam, P. J. Metaxas, and J. Ferré, *Europhys. Lett.* **78**, 57007 (2007).